Frontiers of Materials Science

Electronic Supplementary Material

Preparation of noble metal modified zinc oxide nanoflakes and their gas-sensing properties

Chen Chen[1], Jie Chang (✉)[2], Tao Wang[3], Areeje Fatima[3], Min He (✉)[1], and Jiarui Huang (✉)[3]

1 School of Materials Science and Engineering, Tongling University, Tongling 244000, China
2 Anhui Engineering Research Center of Highly Reactive Micro-Nano Powders, School of Materials and Environmental engineering, Chizhou University, Chizhou 247000, China
3 Key Laboratory of Functional Molecular Solids of the Ministry of Education, Anhui Laboratory of Molecule-Based Materials, College of Chemistry and Materials Science, Anhui Normal University, Wuhu 241002, China

E-mails: changjie@czu.edu.cn (J.C.), 2022009@tlu.edu.cn (M.H.), jrhuang@ahnu.edu.cn (J.H.)

1 Characterizations

Phase composition was conducted using the Shimadzu XRD-6000 X-ray diffractometer (Cu Kα radiation, λ = 1.54178 Å). Field emission scanning electron microscope (FESEM, Hitachi S-4800, accelerating voltage 5 kV) and transmission electron microscope (HRTEM, JEOL-2010, accelerating voltage 200 kV) were used to observe the morphology and microstructure of the materials. The specific surface area and pore size distribution were determined using the Nova 2000E nitrogen adsorption instrument, based on the Barrett–Joyner–Halenda (BJH) model, from the desorption isotherm. X-ray photoelectron spectroscopy (XPS) was performed using Thermo Fisher Nexsa system, equipped with a monochromatic Al Kα light source (1486.6 eV), with an analysis area of 400 μm × 400 μm, an electron emission angle of 90°, and a vacuum pressure below 1×10^{-8} mbar. Samples were analyzed without sputtering or surface etching, with the binding energy calibrated using the surface contamination carbon C 1s peak (284.8 eV). Solid ultraviolet–visible absorption spectra were obtained using the Hitachi UV-Vis-3010 spectrophotometer. Elemental distribution analysis was completed using the energy spectrum attachments of FESEM (Hitachi S-4800, accelerating voltage 15 kV) and HRTEM (JEOL-2010, accelerating voltage 200 kV).

2 Gas sensor fabrication and testing system

Fabrication of gas sensor devices: A certain amount of zinc oxide nanosheet material was mixed with an appropriate amount of anhydrous ethanol to obtain a uniform suspension. The suspension was uniformly coated on the surface of the alumina ceramic tube. A stable coating was obtained after drying. Subsequently, a nickel-chromium heating coil was assembled to the internal channel of the ceramic tube. The fabricated sensor is shown in Fig. S1. In order to enhance the operational stability of the device, the sensors were activated at 280 °C for 48 h, a process that significantly improves the long-term performance of the material.

Gas sensor test system: The test system is constructed based on the principle of steady state gas diffusion, and its working principle is shown in Fig. S2. An electrochemical workstation was used to collect and record, in real time, the resistance changes of the sensor under various gas concentrations. During all gas-sensing tests, the relative humidity in the test chamber was maintained at 37% (RH = 37%) and the ambient temperature was kept at 28 °C (room temperature). To detect gases, a certain amount of various headspace vapors was injected into a 1000 mL of test chamber using a syringe and mixed with air. Some pure gases, such as H_2S, NH_3, CO, and H_2 were used in the gas sensing measurement. All other VOCs vapors, such as ethanol, methanol, acetone, and toluene, came from the headspace vapors of the pure chemical regents at 28 °C under ambient pressure. In this study, the response of the sensor is defined as $S = R_a/R_g$, where R_a and R_g are the resistances of the sensor in air and the target gas, respectively. The response and recovery times were defined as the durations required for the resistance change to reach 90% of its total variation during exposure to or removal from the target gas.

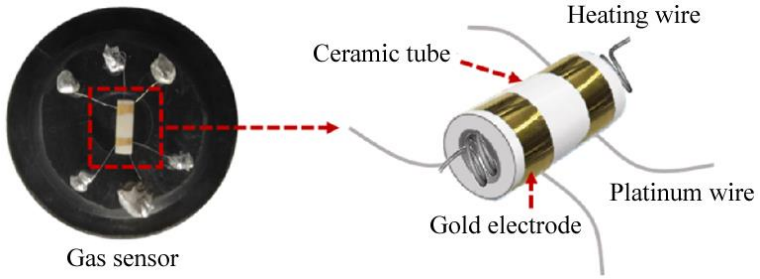

Fig. S1 Schematic diagram of the gas sensor.

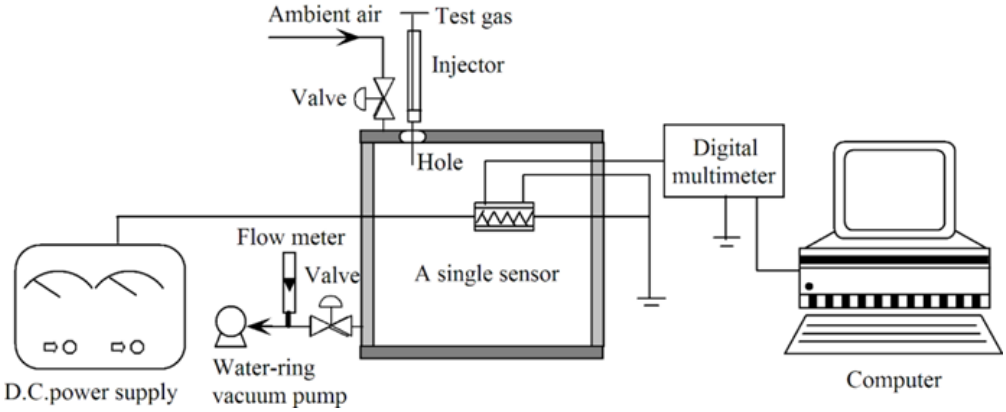

Fig. S2 The sensing test system.

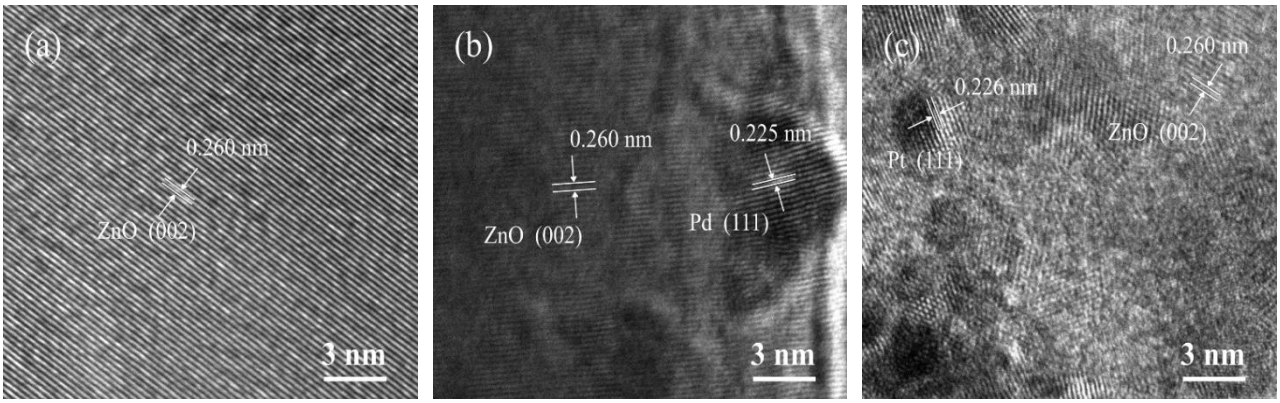

Fig. S3 HRTEM images of **(a)** ZnO, **(b)** Pd/ZnO, and **(c)** Pt/ZnO nanoflakes.

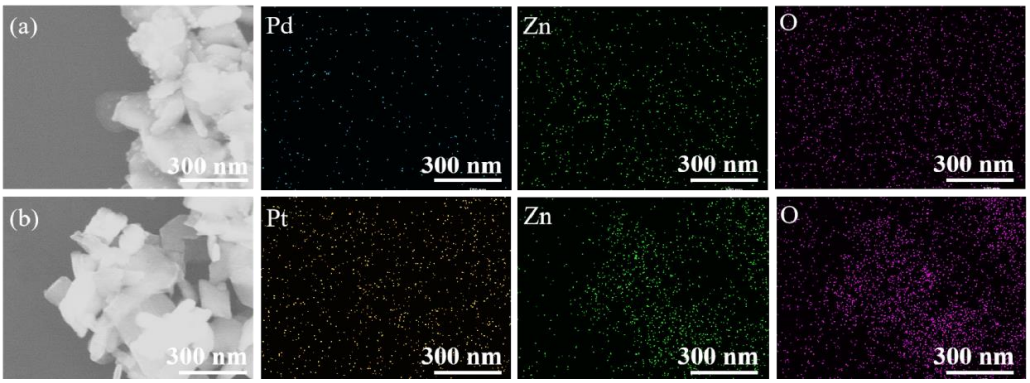

Fig. S4 SEM elemental mapping images of **(a)** Pd/ZnO and **(b)** Pt/ZnO nanoflakes.

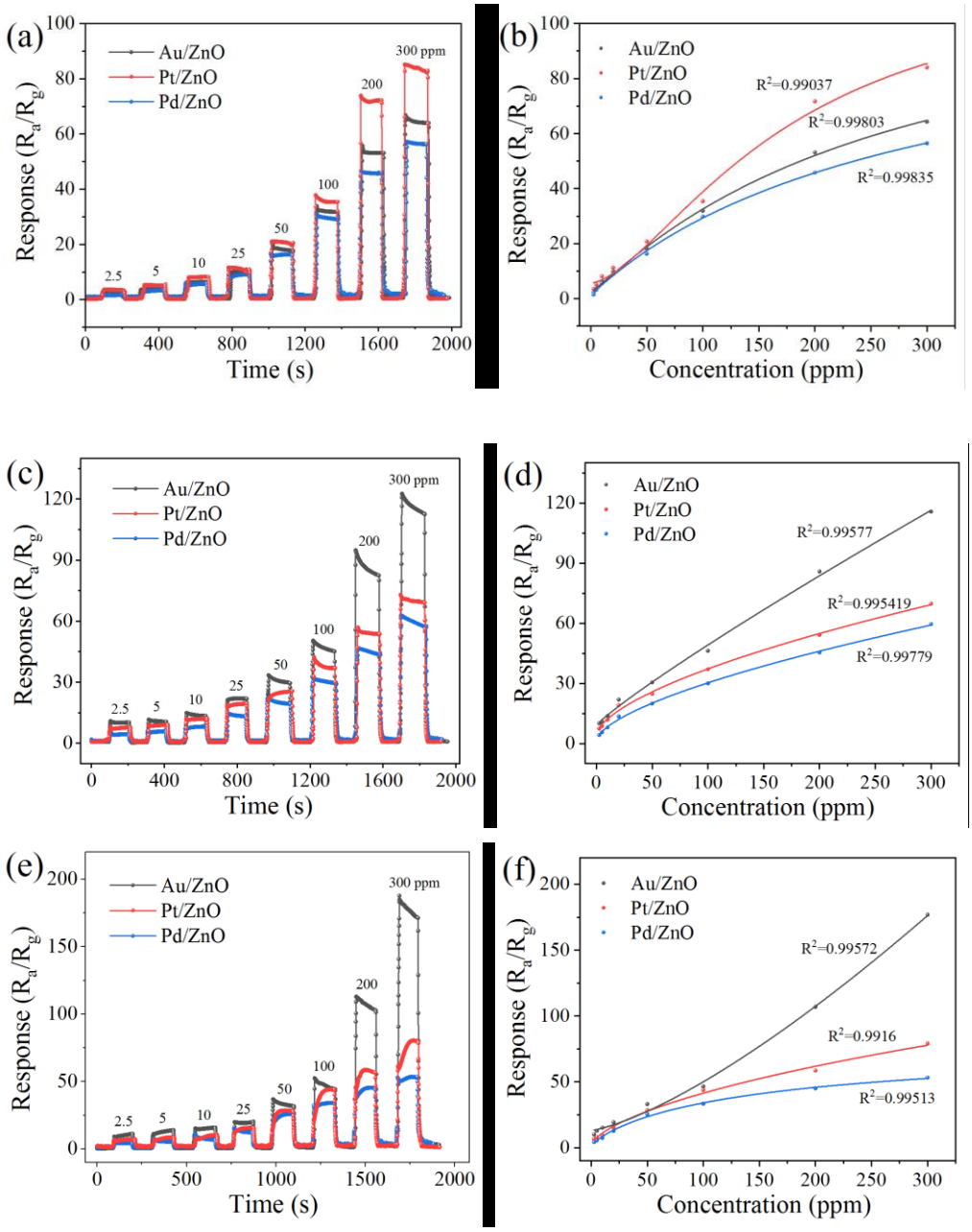

Fig. S5 Transient responses of Au/ZnO, Pt/ZnO, and Pd/ZnO sensors to **(a)** acetone, **(c)** ethanol, and **(e)** n-butanol vapors with various concentrations. Linear relationship between the responses of Au/ZnO, Pt/ZnO, and Pd/ZnO sensors to different concentrations of **(b)** acetone, **(d)** ethanol, and **(f)** n-butanol vapors.

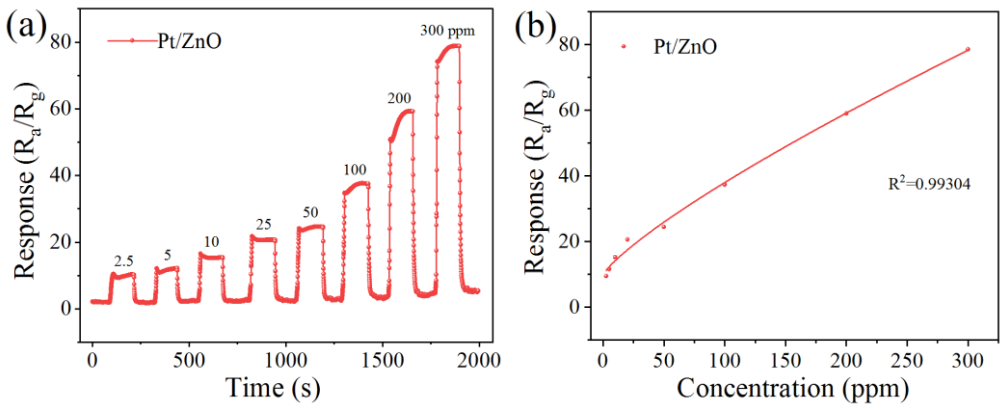

Fig. S6 (a) Transient responses of Pt/ZnO sensor to toluene vapor with different concentrations. **(b)** Linear relationship between the responses of Pt/ZnO sensor to different concentrations of toluene vapor.

Table S1 Comparison of isopropyl alcohol sensing characteristics reported in this paper and those reported in literature

Sensing material	Concentration /ppm	Working temperature/°C	(Response /recovery time)/s	Response	Ref.
Ag–ZnO nanorods	100	320	72/29	27	[25]
Pt/ZnO nanoparticles	100	230	8.7/19.4	91.2	[29]
SnO_2/ZnO core/shell nanocomposites	500	300	26/175	103.3	[26]
Coral-like ZnO–ZrO_2	100	350	19/8	35	[27]
Pt/SnO_2 microflowers	100	180	164/173	14.5	[43]
Pt-doped TiO_2 nanoparticles	100	250	19/10	80	[52]
Au/ZnO nanoflakes	100	225	8/12	132.2	This work